Key Points:
- Comprehensive analysis of global and hemispheric energy exchanges within the Mars atmosphere
- Thermal tides have a significant impact on eddy energy and conversion terms
- Most conversion occurs in zonal component but is canceled out in annual and global mean

Supporting Information:
- Supporting Information S1
- Figure S1
- Figure S2
- Figure S3
- Figure S4
- Figure S5
- Figure S6
- Figure S7
- Text S1
- Text S2

Correspondence to:
F. Tabataba-Vakili,
fachreddin.tabataba-vakili@physics.ox.ac.uk

A Lorenz/Boer energy budget for the atmosphere of Mars from a "reanalysis" of spacecraft observations

Fachreddin Tabataba-Vakili[1], Peter L. Read[1], Stephen R. Lewis[2], Luca Montabone[1,3], Tao Ruan[1], Yixiong Wang[1], Alexandru Valeanu[1], and Roland M. B. Young[1]

[1]Atmospheric, Oceanic and Planetary Physics, Department of Physics, University of Oxford, Oxford, UK, [2]Department of Physical Sciences, Open University, Milton Keynes, UK, [3]Space Science Institute, Boulder, Colorado, USA

Abstract We calculate a Lorenz energy budget for the Martian atmosphere from reanalysis derived from Mars Global Surveyor data for Mars years 24–27. We present global, annual mean energy and conversion rates per unit area and per unit mass and compare these to Earth data. The directions of the energy conversion terms for Mars are similar to Earth, with the exception of the barotropic conversion between zonal and eddy kinetic energy reservoirs. Further, seasonal and hemispheric decomposition reveals a strong conversion between zonal energy reservoirs over the year, but these balance each other out in global and annual mean. On separating the diurnal timescale, the contribution to the conversion terms and eddy kinetic energy for diurnal and shorter timescales in many cases (especially during planet-encircling dust storms) exceeds the contribution of longer timescales. This suggests that thermal tides have a significant effect on the generation of eddy kinetic energy.

1. Introduction

The Lorenz energy budget [*Lorenz*, 1955] is a useful approach commonly used to assess or quantify the pathways by which energy is transferred between different components of kinetic and potential energies, from generation via differential heating to dissipation via friction. Up to now, the Lorenz energy cycle scheme has been most commonly applied to the mean state of the terrestrial atmosphere. Local calculations of Lorenz energy budgets have also been employed, for instance, in studies of the eddy formation mechanism and evolution of cyclones [*Dias Pinto and da Rocha*, 2011], local rainy seasons [*Berry and Thorncroft*, 2012], or northern hemisphere winter jets [*Jiang et al.*, 2013], but such local studies typically require large additional energy transport terms as the boundaries of the studied region are permeable. In the global-mean, energy cycles can be used to analyze discrepancies between reanalysis data sets [e.g., *Oort*, 1983; *Li et al.*, 2007] or to validate model simulations with reanalysis data on the basis of their pattern of energy reservoirs and conversions [e.g., *Boer and Lambert*, 2008; *Marques et al.*, 2011]. Concerning planets other than the Earth, *Lee and Richardson* [2010] computed Lorenz energy budgets from model simulations of Venus to assess the effect of numerical dissipation and the choice of different numerical cores on the superrotation in Venus models. However, in general, such diagnostics have not been widely computed for planets other than the Earth.

A detailed analysis of the Lorenz energy budget via temporal or spatial decomposition of the integrands can give further information on seasonal and even daily atmospheric behavior. Applying the Lorenz energy cycle equations to the Martian atmosphere allows a study of atmospheric energetics under conditions significantly different from those of Earth. The effects of global-scale dust storms, thermal tides, highly variable terrain, and the strong seasonal cycle of Mars on the Lorenz cycle are of particular interest. Moreover, there appears to have been no detailed and complete calculation of the Lorenz energy budget for the Martian atmosphere published until now, although there are studies which have computed some energetics for Mars from global climate model (GCM) simulations [see, e.g., *Haberle et al.*, 1993; *Kavulich et al.*, 2013; *Wang et al.*, 2013]. The availability of complete reanalysis data sets for Mars, such as the Mars Analysis Correction Data Assimilation (MACDA) data set version 1.0 used here [*Montabone et al.*, 2014], offers the possibility of computing an energy budget that is as consistent as possible with observations. In addition, the data presented in this work should provide a relevant set of statistics against which to verify model simulations of the Martian atmosphere.

2. Data Sources and Methods

For our study we use data from the UK Mars reanalysis data set MACDA v1.0 [*Montabone et al.*, 2014] based on the UK spectral version of the Laboratoire de Météorologie Dynamique/The Open University/University of Oxford Mars global climate model (LMD-UK GCM) [*Forget et al.*, 1999]. MACDA uses temperature and dust opacity data derived from infrared spectral data obtained between May 1999 and August 2004 by the Thermal Emission Spectrometer on NASA's Mars Global Surveyor spacecraft [*Christensen et al.*, 2001]. The resulting reanalysis data set resolves complete diurnal cycles (with 2 h time steps) of the Martian atmosphere from solar longitude $L_s = 141°$ in Mars year (MY) 24 to $L_s = 82°$ in MY 27. The solar longitude (L_s) is an angle describing the orbital position of Mars in reference to the northern hemisphere spring equinox at $L_s = 0°$. Other important points are the summer solstice ($L_s = 90°$), autumn equinox ($L_s = 180°$), and winter solstice ($L_s = 270°$), all with respect to the northern hemisphere.

Because Mars is an extremely mountainous planet, we use the energy cycle formulation of *Boer* [1989], who explicitly takes into account finite amplitude topographic variations in his derivation. In general, the Lorenz scheme decomposes energy exchanges into the following schematic form

$$\frac{\partial A_Z}{\partial t} = G_Z - C_Z - C_A \tag{1}$$

$$\frac{\partial A_E}{\partial t} = G_E - C_E + C_A \tag{2}$$

$$\frac{\partial K_Z}{\partial t} = C_Z - C_K - F_Z \tag{3}$$

$$\frac{\partial K_E}{\partial t} = C_E + C_K - F_E, \tag{4}$$

which describe the generation G of available potential energy (APE) A, decomposed into zonal (A_Z) and eddy (A_E) terms. Both A_Z and A_E are converted into kinetic energies K_Z and K_E, which are then dissipated due to frictional processes F_Z and F_E. Conversion C between all four energy terms is described by $C_Z(A_Z \rightarrow K_Z)$, $C_E(A_E \rightarrow K_E)$, $C_A(A_Z \rightarrow A_E)$, and $C_K(K_Z \rightarrow K_E)$. Note that the C_K defined in this scheme is in the opposite direction to the formulation by, e.g., *Peixóto and Oort* [1974].

The Lorenz cycle equations used here were derived by *Boer* [1989] from the hydrostatic primitive equations without further approximation (such as quasigeostrophic or flat surface approximations as in, e.g., *Peixóto and Oort* [1974] and *Lorenz* [1955]) and are hence termed "exact" equations. The additional effect of directly including topography produces extra terms in A_E, A_Z, C_K, and C_Z when compared to more approximated formulations [see, e.g., *Peixóto and Oort*, 1974; *Lorenz*, 1955; *James*, 1995]. These additional terms are labeled with a subscript "$_2$" in the current work, while the terms that are more comparable to the conventional approximated equations are indicated with a subscript "$_1$". The additional terms A_{E2}, A_{Z2}, and C_{Z2} are integrals over the surface area of the planet, and C_{K2} can be interpreted as a material rate of change of the potential energy (see supporting information for the full equations) [*Boer*, 1989].

Another difference between the formulation of *Boer* [1989], which is used here, and conventional formulations is the usage of the efficiency factor $N(\pi)$ in computing APE terms (see supporting information). Using N to determine APE terms has a significant impact compared to the more conventional approximate APE determination, since N can assume negative values [see, e.g., *Boer*, 1975; *Lorenz*, 1955; *Siegmund*, 1994]. The efficiency factor requires an explicit determination of the reference state of the atmosphere, which is the state of the atmosphere where available potential energy is minimal. We calculate this reference state via a terrain-dependent determination method presented by *Koehler* [1986].

Using the *Boer* [1989] scheme, we can compute energy and conversion terms separately for each time step. These terms are then temporally averaged over 30 Martian mean solar days (sols). The generation G and dissipation F terms are determined from the residuals of the conversion terms in global and annual means.

The general interpretation of the Lorenz energy cycle of the terrestrial atmosphere is that C_Z signifies the strength of axisymmetric circulation such as the Hadley circulation. Conversion from A_Z to A_E to K_E is associated with baroclinic instabilities, and conversion from K_Z to K_E can be related to barotropic instability [see, e.g., *James*, 1995]. Alternatively, a conversion of K_E to K_Z signifies the generation of zonal flows through mechanical
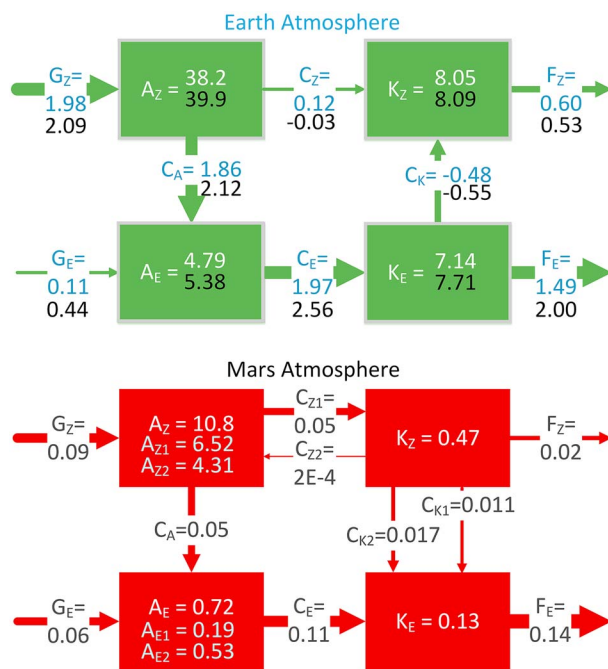
Figure 1. Mean values of energy and conversion terms per unit area (top) of Earth [*Boer and Lambert*, 2008] from National Centers for Environmental Prediction (NCEP) (white/blue) and ERA (black) reanalysis data over 17 years (1979–1995) and (bottom) of Mars over almost 3 Martian years (current work) . All energies (A_Z, A_E, K_Z, K_E) are given in $10^5 \, \mathrm{J \, m^{-2}}$ and all conversion terms in $\mathrm{W \, m^{-2}}$.

eddy forcing. Figure 1 (top) shows the global and annual mean Lorenz energy cycle of Earth [*Boer and Lambert*, 2008], which will be compared to that of Mars in section 3.1.

The planet Mars is in many ways very different from Earth. Its very thin atmosphere and lack of surface oceans, together with its higher orbital eccentricity and obliquity, makes Mars much more susceptible to seasonal changes. This manifests itself during solstices in the formation of strong equator-crossing Hadley cells. Seasonal effects in both hemispheres are studied in section 3.2. Another phenomenon specific to the Martian atmosphere is the strong activity of thermal tides [*Zurek*, 1976; *Wilson and Hamilton*, 1996]. Accordingly, we use a diurnal filter to evaluate separately the effects of diurnal tides and other transient eddies on the energy budget in section 3.3.

In addition, Mars has an enhanced dust storm season in the second half of the year, during which both regional and global-scale dust storms may occur.

Roughly every one in three Mars years a global-scale dust storm event (GDSE) occurs [*Zurek and Martin*, 1993; *Mulholland et al.*, 2013], which commonly lasts up to a hundred sols. In our available data set, there is one such event starting from $L_s \approx 185°$ in MY 25. In years without GDSEs the annual climate of Mars shows repetitive patterns [see, e.g., *Liu et al.*, 2003; *Smith*, 2004] in surface temperature, dust, water ice, and water vapor observations. Having almost 3 years of Mars reanalysis data to produce our atmospheric energy budgets is likely much less of a disadvantage than it would be for Earth when considering the above climatological averages, at least outside the main GDSE period.

3. Results

3.1. Global Budget

Figure 1 shows schematic global and annual mean Lorenz energy budgets for both Earth and Mars. The Earth data were taken from a previous energy cycle analysis computed from NCEP reanalysis data over 17 years (1979–1995) by *Boer and Lambert* [2008, Table 4]. Their analysis used the approximated Lorenz energy scheme of *Peixóto and Oort* [1974]. While it would be ideal to compare our Mars results to Earth values computed with the same scheme, such data were not available. However, the scheme used for the Earth data [*Boer and Lambert*, 2008] has terms that are, in general, comparable to the terms used in the current work when excluding terms labeled "$_2$". These terms vanish in the flat surface approximation [*Boer*, 1989], suggesting that they are less important for the comparatively flat topography of Earth.

The energy and conversion term values per unit area for Mars (Figure 1, bottom) are significantly smaller than for Earth. When considering the rate of generation G_Z, G_E of available potential energy (APE) via diabatic heating, lower values per unit area are to be expected for Mars, since it firstly receives less solar irradiance compared to Earth due to its larger orbital distance and secondly, Mars' atmosphere is less dense and consequently has a smaller column-integrated mass. The direct generation of eddy APE (G_E) gains in importance on Mars, as the ratio $G_E/G_Z(\mathrm{Mars}) = 0.5$ is larger than the corresponding Earth value.

The atmospheric energy reservoirs per unit area A_Z, A_E, K_Z, and K_E are also lower than on Earth. The additional surface-related energy terms, A_{Z2} and A_{E2}, provide a significant contribution to the total energy reservoir. In

the case of A_E, A_{E2} even outweighs A_{E1} by a factor of 5. This shows that the Martian surface is uneven enough to require the inclusion of surface terms to the energy equations.

The conversion terms per unit area (C_A, C_E, C_K, C_Z) on Mars are again small compared to Earth, but both budgets seem to favor baroclinic conversion from A_Z to A_E to K_E. The direction of C_K, however, is in the opposite sense for Earth and Mars (see Figure 1). The negative (K_E to K_Z) value of C_K for Earth indicates that eddies strengthen the zonal flow, whereas on Mars the positive values of C_K can be associated with a weakening of the zonal flow. Note that C_{K2} contributes roughly 60% to the total C_K. When comparing C_Z to the dominant conversion terms (C_A, C_K) of each respective planet, Martian C_Z has a larger relative impact on the total budget than its terrestrial counterpart (see section 3.2 for details). Overall, this means that on Mars two significant pathways of energy conversion can be observed in the global mean: (1) a strong baroclinic conversion from A_Z to A_E to K_E, which is also the dominant pathway for Earth and (2) a weaker conversion pathway from A_Z to K_Z to K_E. The frictional dissipation terms on Mars and Earth seem to favor dissipation mainly in the eddy component.

When we compute the energy and conversion terms in units per kilogram (by dividing by p_0/g, where p_0 is the reference surface pressure of the respective planet and g is the respective planetary gravitational acceleration), Mars values become larger than those of Earth (see Figure S2). This difference can be explained via the generation of energy due to solar input. The atmospheric density of Mars is 75 times less than that of Earth, while the solar irradiation is 2.3 times less, which makes the Mars atmosphere roughly 33 times more susceptible to solar forcing [*Tyler and Barnes*, 2013]. However, instead of this factor, we only see an increase by a factor of around 3 when comparing $G = G_Z + G_E$ of Mars and Earth. This difference is likely due to differences in the absorption of energy by the atmospheric constituents, which are higher for Earth compared to the mostly transparent CO_2 on Mars. When taking these factors into account, the decreased density of the Mars atmosphere seems to outweigh other factors, producing larger energy and conversion terms per unit mass.

Further decompositions in time and space are presented below to further understand seasonal and diurnal effects on the Martian Lorenz energy cycle.

3.2. Hemispheric and Seasonal Decomposition

The energy cycle of an open domain such as a hemisphere is no longer in equilibrium unless additional surface and boundary terms are taken into account. While ignoring these terms disregards local equilibrium, one can still learn about the transfer of energy between these open domains. In particular, the partition into northern and southern hemispheres (NH and SH) can be helpful in understanding the atmospheric energy cycle during different seasons [see, e.g., *Li et al.*, 2007] as well as the role of the cross-equator Hadley circulation of Mars. From here on, we do not calculate generation and dissipation terms from the residuals as integration times may be too short to be able to assume atmospheric equilibrium.

Figure 2 shows data for all energies and conversion terms of the Lorenz energy cycle for the NH, SH, and the whole globe in annual and seasonal mean for the four main cardinal seasons. The seasons depicted are centered about the solstices and equinoxes (for values bounded by solstices/equinoxes see Table S1). The energy reservoirs exhibit different responses to the changing seasons. Zonal energy terms in each hemisphere show a direct dependence on the season so that the summer/winter hemisphere has a dominating contribution to A_Z/K_Z. Overall, the zonal energies are stronger in the northern hemisphere, except during the solstices where the SH contribution to A_Z and K_Z dominates in its respective summer or winter. The difference in hemispheric energies is likely related to the surface dichotomy and the difference of energy throughput during the aphelion/perihelion cycle. Regarding the eddy terms, K_E shows equal contribution from both hemispheres but with yearly modulated total values. A_E evidently decreases during solstices in the NH, whereas SH values are mostly constant over the year. The diurnal component of the hemispheric energies suggests that in the SH synoptic and diurnal scale A_E compensate each other while this does not occur in the NH.

The hemispheric decomposition of C_{Z1} in Figure 2 reveals large values with opposing signs. While positive C_{Z1} values are indicative of a thermally direct circulation, negative values are associated with thermally indirect circulation [*Lorenz*, 1967]. Accordingly, we find that the circulation in summer solstice hemispheres is thermally direct, whereas that of winter solstice hemispheres is thermally indirect. The overall hemispheric strength of this conversion is 4 times stronger in southern summer than in northern summer. This result is in accordance with *Richardson and Wilson* [2002], who concluded that asymmetries in the topography of Mars favor a predominating southern summer circulation. It is interesting to note that the hemispheric values of C_{Z1} nearly cancel each other out. This can be accounted for by a strong winter hemisphere Ferrel-like circulation as well
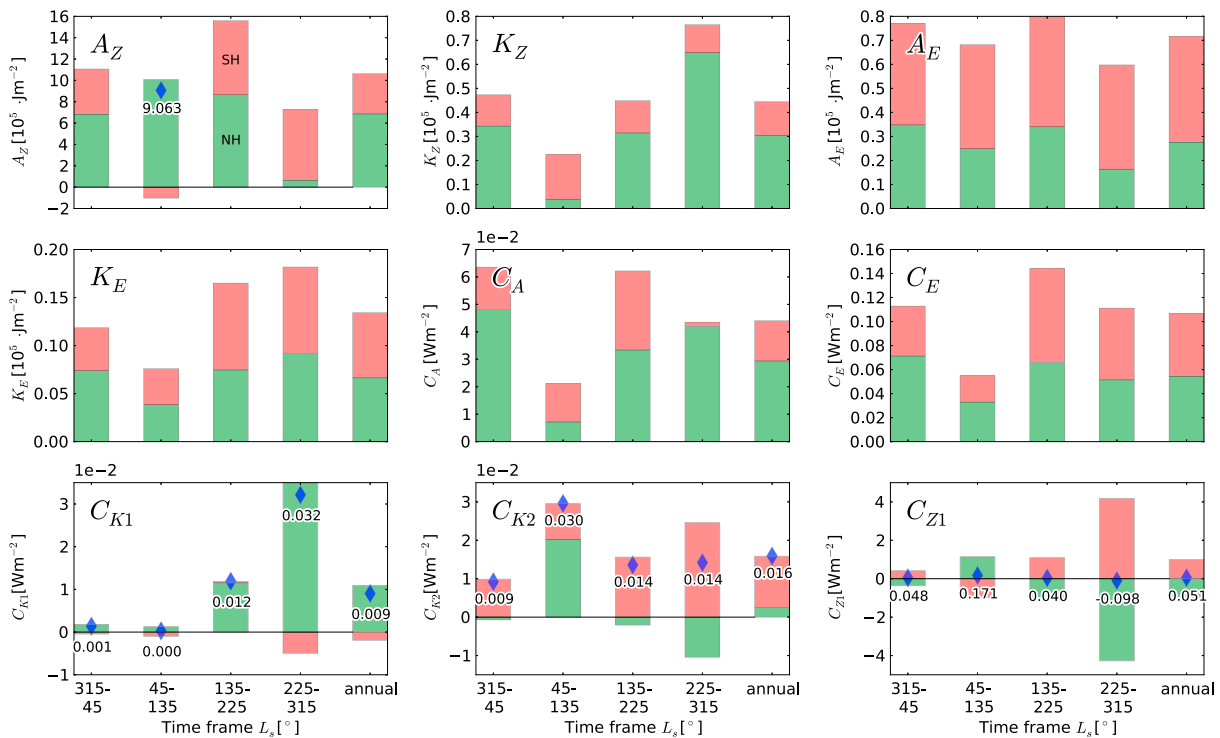
Figure 2. Lorenz energy budget of Mars in seasonal and hemispheric decomposition. Global values are given by the sum of northern (green) and southern (red) hemisphere contribution or by a blue diamond where given. Seasons are given in solar longitudes, where $L_s = 0°$ is the northern hemisphere spring equinox. Annual values were averaged over two full years (MY 25 and MY 26). Seasonal values are the mean of either two ($L_s = 45–135°$) or three ($L_s = 135–225°$, $225–315°$, $315–345°$) years of data.

as the heating induced by compression in the downward branch of the cross-equatorial Hadley circulation [see, e.g., *Haberle et al.*, 1993].

On global scales both C_A and C_E are highest during equinoxes. During solstices (especially during the northern winter solstice, $L_s = 45–135°$) this baroclinic conversion decreases (see section 3.3).

Regarding the conversions with additional terms (C_{K2}, C_{Z2}), we find that C_Z is dominated by C_{Z1} and that C_{Z2} is negligible (see Table S1). For C_K, however, both terms have significant contributions. During NH winter C_K is dominated by C_{K1}, converting K_Z to K_E, whereas C_{K2} is stronger during the summer of each hemisphere.

3.3. Diurnal and Synoptic Frequency Components

In this section, time-resolved values of the Lorenz energy cycle terms, each represented by X, are computed to investigate variations in atmospheric energy conversions for instance during the global-scale dust storm of MY 25. In addition, we filter out the diurnal component of each term to assess the importance of the diurnal tides to the energy conversion within the Martian atmosphere relative to other components of the circulation. The filtering was performed by taking the daily running mean (i.e., averaging over the length 1 day) of all input variables and then computing the daily-averaged Lorenz energy cycle terms $\overline{X}$. The diurnal component X_{diurnal} of each term, representing the contribution from periods equal to or shorter than the diurnal period, is then computed from

$$X = \overline{X} + X_{\text{diurnal}} .\tag{5}$$

Figure 3 depicts (a) total X, (b) daily-mean $\overline{X}$, and (c) the diurnal values X_{diurnal} of the conversion terms with each data point representing a time frame of 30 sols. C_Z shows a strong yearly repetition, being positive in NH spring and summer and negative in NH autumn and winter. This behavior is in accordance with a change between thermally indirect and direct circulations. We separate C_{K1} and C_{K2} in this instance to further study the contribution to C_K in seasonal decomposition. In the global mean, C_{K1} assumes positive values from $L_s = 180°$ to $L_s = 360°$, while C_{K2} assumes values between 1 and 2 mW m^{-2} over the whole year. At $L_s = 180°$ of MY 25, there is first a positive (K_Z to K_E) peak in C_{K1} followed closely by a small negative peak (originating from the SH,
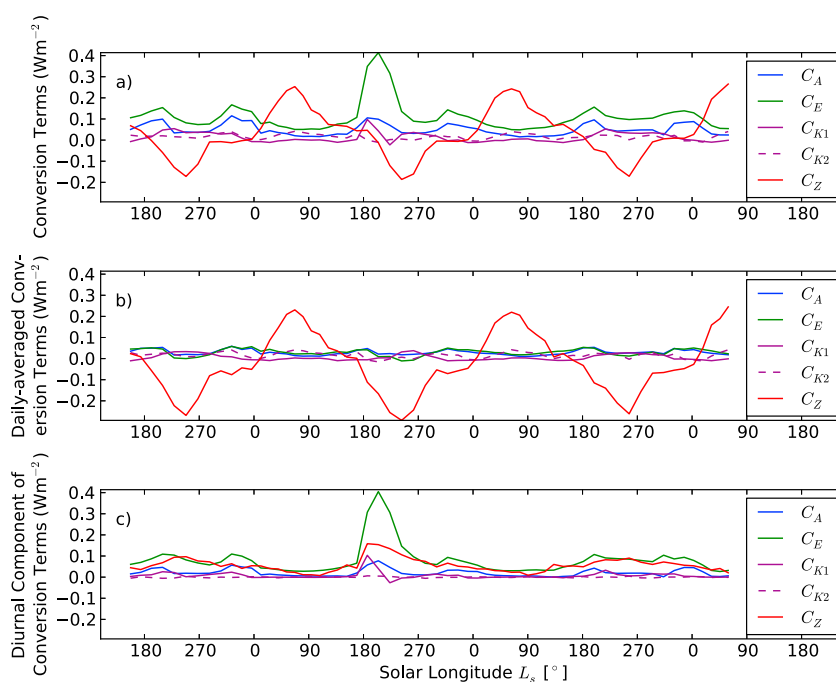
Figure 3. (a) Total X, (b) daily-averaged $\overline{X}$, (c) and diurnal X_{diurnal} components of the conversion terms of the Lorenz energy budget of the Mars atmosphere given in 30 sol mean values from $L_s = 141°$ MY 24 to $L_s = 82°$ MY 27.

see Figure S7). Even more striking is a large spike in C_E at around $L_s = 180 - 270°$ of MY 25. The K_E reservoir also increased during that time (see Figure S3). This behavior is coincident in time with the GDSE that occurred during $L_s = 180 - 240°$ of MY 25 [cf. *Lewis and Barker*, 2005, Figure 5].

The daily-averaged (Figure 3b) and diurnal (Figure 3c) components show which conversions take place on timescales longer and shorter than 1 sol, respectively. We find that most zonal conversion (C_Z) occurs on longer timescales, apart from a small offset that is generated at the equatorial surface region (see Figure S5). Hemispheric decompositions of Figure 3 (see Figures S6 and S7) show that an overwhelming zonal conversion with up to 10 W m^{-2} occurs on longer than daily timescales, but these larger values are largely balanced in the global mean (Figure 3). A small amount of baroclinic conversion (C_A, C_E) also occurs on longer timescales. Apart from C_{K2} all conversion terms exhibit nonnegligible diurnal components (Figure 3c). While the offset between total and daily-averaged C_Z provides comparable values to the other diurnal conversions, it represents only a small fraction of zonal conversion compared with the hemispheric C_Z values discussed above. A latitude pressure plot of the diurnal component of the integrands of C_Z (see Figure S5) reveals that diurnal C_Z occurs near the equatorial surface, which can be either associated with the diurnally modulated upslope and downslope winds or with the generation of zonal flows by tidal interactions [*Lewis and Read*, 2003].

Most diurnal conversion terms assume their maximum values during the GDSE. This behavior shows that dust storms on Mars are strongly correlated with diurnal effects such as thermal tides and coincide with both baroclinic and barotropic conversions noticeably increasing K_E production. This correlation between dust storms and thermal tides has been shown by *Leovy and Zurek* [1979] using observations of pressure oscillations measured by the Viking I and II landers. In addition, *Lewis and Barker* [2005] investigated variations of thermal tides in an assimilated reanalysis of the same period as discussed here and found mainly semidiurnal signatures during the global-scale dust storm in MY 25.

During the northern winter solstice (around $L_s = 270°$, see Figures 3a, 3b, and S6) we also see a decrease in baroclinic activity (C_A, C_E), which coincides with an increase in barotropic conversion. This behavior coincides with the "solsticial pause," where transient eddy activity is strong before and after the winter solstice but decreases during this time span [*Read et al.*, 2011; *Wang et al.*, 2013; *Kavulich et al.*, 2013; *Lewis et al.*, 2015; *Mulholland et al.*, 2015].
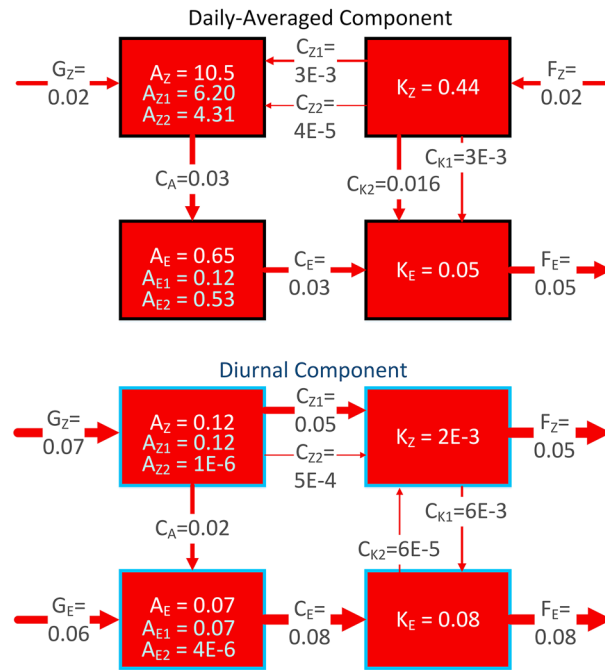
Figure 4. Global and annual mean values of (top) daily-averaged and (bottom) diurnal components of energy and conversion terms per unit area of Mars over 2 full Mars years. All Energies (A_Z, A_E, K_Z, K_E) are given in 10^5 J m^{-2} and all conversion terms in W m^{-2}.

Regarding the energy reservoirs (see Figure S3), eddy energy terms have substantial amplitudes in their diurnally varying components. A_E shows seasonally recurring contributions of up to 25% during $L_s = 180–360°$ (northern spring/summer and dust season) and negligibly small amounts during the other half of the year. Moreover, the diurnal component of K_E contributes over 50% of its total value. This contribution rises to 90% during the global-scale dust storm event of MY 25. Diurnal contributions to zonal energies are negligible.

Figure 4 (bottom) summarizes the importance of the diurnal components, by showing their global and annual mean values per unit area. When compared with the daily-averaged values from Figure 4 (top), we see that overall the conversion terms C_E, C_{K1}, and C_A are controlled on diurnal and shorter timescales, favoring the production of K_E. In addition, in annual mean 10% of the A_E and 50% of the K_E reservoir resides on such timescales. Additionally, direct generation of eddy and zonal APE (G_Z, G_E) seems to be strong in the diurnal components but weak in the more slowly varying components. Note also the reversal of C_Z between Figure 4 (top and bottom), suggesting that the global and annual circulation behaves in a thermally direct sense in the diurnal component and slightly indirect on longer timescales.

4. Conclusion

We have computed both global and temporal means as well as seasonal, diurnal, and hemispheric components of the Lorenz energy cycle of the Martian atmosphere during Mars years 24 to 27. In global and temporal means the Martian atmosphere shares many of the overall characteristics of Earth's Lorenz energy cycle. Important differences can be observed when decomposing the integrands, however, most notably the opposing signs in the conversion between kinetic energy reservoirs, which reveals a barotropically unstable contribution to eddy generation in the Martian atmosphere. This difference implies that on Mars there isn't the same tendency for upscale energy transfer as observed on Earth with regard to the eddy, zonal flow interaction. When including the surface topography in the derivation of the Lorenz energy equations for Mars, essential contributions to A_E, A_Z, and C_K can be observed from the additionally arising terms in the "exact" budget equations [see *Boer*, 1989].

Hemispheric decomposition of C_Z reveals a large seasonal variation between thermally direct and indirect heating mechanisms. We have also found that zonal energy terms are dependent on the season of their hemisphere, whereas eddy kinetic energy changes globally and has its maximum during southern hemisphere summer apparently following the aphelion/perihelion cycle.

Filtering out diurnal and smaller timescales shows that thermal tides provide an important contribution to the conversion of energy in the Martian atmosphere. The generation of kinetic eddy energy K_E via C_E and C_K occurs predominantly on such timescales. During global-scale dust storm events K_E increases considerably, of which 90% can be attributed to processes that operate on diurnal and smaller timescales such as thermal tides.

References

Berry, G. J., and C. D. Thorncroft (2012), African easterly wave dynamics in a mesoscale numerical model: The upscale role of convection, *J. Atmos. Sci.*, *69*(4), 1267–1283.

Boer, G. J. (1975), Zonal and eddy forms of the available potential energy equations in pressure coordinates, *Tellus*, *27*(5), 433–442.

Boer, G. J. (1989), On exact and approximate energy equations in pressure coordinates, *Tellus A*, *41*(2), 97–108.

Boer, G. J., and S. Lambert (2008), The energy cycle in atmospheric models, *Clim. Dyn.*, *30*(4), 371–390.

Christensen, P. R., et al. (2001), Mars global surveyor thermal emission spectrometer experiment: Investigation description and surface science results, *J. Geophys. Res.*, *106*(E10), 23,823–23,871.

Dias Pinto, J. R., and R. P. da Rocha (2011), The energy cycle and structural evolution of cyclones over southeastern South America in three case studies, *J. Geophys. Res.*, *116*, D14112, doi:10.1029/2011JD016217.

Forget, F., F. Hourdin, R. Fournier, C. Hourdin, O. Talagrand, M. Collins, S. R. Lewis, P. L. Read, and J.-P. Huot (1999), Improved general circulation models of the Martian atmosphere from the surface to above 80 km, *J. Geophys. Res.*, *104*(E10), 24,155–24,175.

Haberle, R. M., J. B. Pollack, J. R. Barnes, R. W. Zurek, C. B. Leovy, J. R. Murphy, H. Lee, and J. Schaeffer (1993), Mars atmospheric dynamics as simulated by the NASA Ames general circulation model: 1. The zonal-mean circulation, *J. Geophys. Res.*, *98*(E2), 3093–3123.

James, I. N. (1995), *Introduction to Circulating Atmospheres*, Cambridge Univ. Press, Cambridge, U. K.

Jiang, T., Y. Deng, and W. Li (2013), Local kinetic energy budget of high-frequency and intermediate-frequency eddies: Winter climatology and interannual variability, *Clim. Dyn.*, *41*(3–4), 961–976.

Kavulich, M. J., I. Szunyogh, G. Gyarmati, and R. J. Wilson (2013), Local dynamics of baroclinic waves in the Martian atmosphere, *J. Atmos. Sci.*, *70*(11), 3415–3447.

Koehler, T. L. (1986), A terrain-dependent reference atmosphere determination method for available potential energy calculations, *Tellus A*, *38*(1), 42–48.

Lee, C., and M. Richardson (2010), A general circulation model ensemble study of the atmospheric circulation of Venus, *J. Geophys. Res.*, *115*, E04002, doi:10.1029/2009JE003490.

Leovy, C. B., and R. W. Zurek (1979), Thermal tides and Martian dust storms: Direct evidence for coupling, *J. Geophys. Res.*, *84*(B6), 2956–2968.

Lewis, S. R., and P. R. Barker (2005), Atmospheric tides in a Mars general circulation model with data assimilation, *Adv. Space Res.*, *36*(11), 2162–2168.

Lewis, S. R., and P. L. Read (2003), Equatorial jets in the dusty Martian atmosphere, *J. Geophys. Res.*, *108*(E4), 5034, doi:10.1029/2002JE001933.

Lewis, S. R., D. P. Mulholland, P. L. Read, L. Montabone, R. J. Wilson, and M. D. Smith (2015), The solsticial pause on Mars: 1. A planetary wave reanalysis, *Icarus*, doi:10.1016/j.icarus.2015.08.039.

Li, L., A. P. Ingersoll, X. Jiang, D. Feldman, and Y. L. Yung (2007), Lorenz energy cycle of the global atmosphere based on reanalysis datasets, *Geophys. Res. Lett.*, *34*, L16813, doi:10.1029/2007GL029985.

Liu, J., M. I. Richardson, and R. J. Wilson (2003), An assessment of the global, seasonal, and interannual spacecraft record of Martian climate in the thermal infrared, *J. Geophys. Res.*, *108*(E8), 5089, doi:10.1029/2002JE001921.

Lorenz, E. N. (1955), Available potential energy and the maintenance of the general circulation, *Tellus*, *7*(2), 157–167.

Lorenz, E. N. (1967), *The Nature and Theory of the General Circulation of the Atmosphere*, World Meteorological Organization, Geneva, Switz.

Marques, C. A. F., A. Rocha, and J. Corte-Real (2011), Global diagnostic energetics of five state-of-the-art climate models, *Clim. Dyn.*, *36*(9–10), 1767–1794.

Montabone, L., K. Marsh, S. R. Lewis, P. L. Read, M. D. Smith, J. Holmes, A. Spiga, D. Lowe, and A. Pamment (2014), The Mars Analysis Correction Data Assimilation (MACDA) dataset v1. 0, *Geosci. Data J.*, *1*(2), 129–139.

Mulholland, D. P., P. L. Read, and S. R. Lewis (2013), Simulating the interannual variability of major dust storms on Mars using variable lifting thresholds, *Icarus*, *223*(1), 344–358.

Mulholland, D. P., S. R. Lewis, P. L. Read, J.-B. Madeleine, and F. Forget (2015), The solsticial pause on Mars: 2. Modelling and investigation of causes, *Icarus*, doi:10.1016/j.icarus.2015.08.038.

Oort, A. H. (1983), Global atmospheric circulation statistics, 1958–1973, *NOAA Prof. Pap. 14*, U.S. Gov. Print. Off., Washington, D. C.

Peixóto, J. P., and A. H. Oort (1974), The annual distribution of atmospheric energy on a planetary scale, *J. Geophys. Res.*, *79*(15), 2149–2159.

Read, P., L. Montabone, D. Mulholland, S. Lewis, B. Cantor, and R. Wilson (2011), Midwinter suppression of baroclinic storm activity on Mars: Observations and models, in *Fourth International Workshop: Mars Atmosphere Modelling and Observations, 8–11 February 2011, Paris, France*, edited by F. Forget and E. Millour, pp. 133–135.

Richardson, M. I., and R. J. Wilson (2002), A topographically forced asymmetry in the Martian circulation and climate, *Nature*, *416*(6878), 298–301.

Siegmund, P. (1994), The generation of available potential energy, according to Lorenz exact and approximate equations, *Tellus A*, *46*(5), 566–582.

Smith, M. D. (2004), Interannual variability in TES atmospheric observations of Mars during 1999–2003, *Icarus*, *167*(1), 148–165.

Tyler, D., Jr., and J. R. Barnes (2013), Mesoscale modeling of the circulation in the gale crater region: An investigation into the complex forcing of convective boundary layer depths, *Mars*, *8*, 58–77.

Wang, H., M. I. Richardson, A. D. Toigo, and C. E. Newman (2013), Zonal wavenumber three traveling waves in the northern hemisphere of Mars simulated with a general circulation model, *Icarus*, *223*(2), 654–676.

Wilson, R. J., and K. Hamilton (1996), Comprehensive model simulation of thermal tides in the Martian atmosphere, *J. Atmos. Sci.*, *53*(9), 1290–1326.

Zurek, R. W. (1976), Diurnal tide in the Martian atmosphere, *J. Atmos. Sci.*, *33*(2), 321–337.

Zurek, R. W., and L. J. Martin (1993), Interannual variability of planet-encircling dust storms on Mars, *J. Geophys. Res.*, *98*(E2), 3247–3259.